Virtual screening of approved clinic drugs with main protease （3CL^{pro}）reveals potential inhibitory effects on SARS-CoV-2

Qiang Wang[abcde1], Ying Zhao[abcde1], Xiaojia Chen[abcde*]， An Hong[abcde*]

[a]*Institute of Biomedicine & Department of cell Biology, Jinan University, Guangzhou 510632, China.*

[b]*National Engineering Research Center of Genetic Medicine, Guangzhou 510632, China.*

[c]*Guangdong Provincial Key Laboratory of Bioengineering Medicine, Guangzhou 510632, China.*

[d]*Guangdong provincial Engineering Research Center of Biotechnology, Guangzhou 510632, China.*

[e]*Engineering Research Center of Genetic Medicine of Ministry of Education, Guangzhou 510632, China.*

*Corresponding authors: An Hong, tha@jnu.edu.cn; Xiaojia Chen, tchenxj@jnu.edu.cn

[1] Both Qiang Wang and Ying Zhao have contributed to the work equally.

Abstract $3CL^{pro}$ is the main protease of the novel coronavirus (SARS-CoV-2) responsible for their intracellular duplication. Based on virtual screening technology, we found 23 approved clinical drugs such as Carfilzomib, Saquinavir, Thymopentin and etc., which showed high affinity with the $3CL^{pro}$ active sites. These findings suggest that $3CL^{pro}$ inhibitors might be potential candidates for further activity detection and molecular modification.

Keywords SARS-CoV-2; $3CL^{pro}$; Approved drugs; Virtual screening

1. Introduction

A novel coronavirus (SARS-CoV-2) has been identified as the pathogen of the coronavirus pneumonia (COVID-19) which has broken out in Wuhan, China in 2019. The coronavirus has spread globally because of its characteristics of strong contagion and high concealment, but there is no effective and specific antiviral therapy up to now. Currently clinical treatments are suggested with known drugs such as Remdesivir and Chloroquine [1-3]. Lopinavir and ritonavir used to treat HIV infection showed anti-CoV effect *in vitro* and are being tried for clinical treatment of COVID-19 [4-8]. Hence, it is a good strategy to discover anti-COVID-19 drugs from approved drug libraries for it can dramatically shorten development time.

SARS-CoV-2 belonging to beta coronavirus has an envelope and sense single-stranded RNA [9, 10]. It contains four non-structural proteins: 3-chymotry psin-like ($3CL^{pro}$), papain-like protease (PL^{pro}), helicase, and RNA polymerase

[11]. Both $3CL^{pro}$ and PL^{pro} are involved in transcription and replication of the virus. Inhibitors targeting viral proteases have shown anti-coronal virus activity *in vitro* [12, 13]. Among them, the $3CL^{pro}$ is the main protease that plays a key role in the replication cycle of the virus [14]. The protease cleaves pp1a and pp1ab which encoded by the virus ORF1a / b , and they have 96% sequence similarity with the $3CL^{pro}$ of the SARS-CoV that caused an outbreak in 2003 [11, 15].

Coronavirus protease inhibitors show antiviral activity *in vitro*. In this study, we used high-throughput virtual screening technology to discover potential drugs targeting the $3CL^{pro}$ of SARS-CoV-2 from approved drug library and the obtained candidates might be potential inhibitors for further activity detection and molecular modification.

2. Materials and Methods

2.1 Homologous modeling and protein structure alignment

Crystal structures of the 3CLpro of both SARS-CoV-2 and SARS-CoV were obtained from Protein Data Bank (https://www.rcsb.org/). The $3CL^{pro}$ structure file (PDB ID: 6LU7) of SARS-CoV-2 has a resolution of 2.16Å and the $3CL^{pro}$ structure file (PDB ID:2Z9J) of SARS-CoV has a resolution of 1.95Å [16]. The protein sequences (YP_009725301.1 and NP_828863.1) were obtained from NCBI. Homologous modeling of $3CL^{pro}$ of SARS-CoV-2 was performed by using 2Z9J as a template and the SWISS-MODEL online server [17, 18]. The VMD RMSD tool was used to calculate the root mean square deviation (RMSD) of this

model from the $3CL^{pro}$ crystal structure of SARS-CoV-2 [19].

2.2 Virtual screening of $3CL^{pro}$ active regions of SARS-CoV-2.

Prepare the $3CL^{pro}$ crystal structure file (PDB ID: 6LU7). Structural coordinates included $3CL^{pro}$, ligand N3 and water molecules. The step of protein pretreatment was performed by removing ligands and crystal water, then adding hydrogen atoms according to the amino acid protonation state at pH 7.0.

Approved drug library containing 5903 molecules was obtained from ZINC15 (http://zinc15.docking.org/) [20].

Molecular docking was performed by using LeDock software (http://www.lephar.com/). This method was based on a combination of simulated annealing and genetic algorithm to optimize the position and orientation of the ligands. And score given was based on physical and empirical methods [21]. The putative catalytic dyad (Cys-145 and His-41) and substrate binding pocket regions were selected as docking regions in this protease [22]. Binding energy was calculated by molecular docking of the receptor protein with each drug and sequencing by their scores. The molecules with binding energy less than -11kcal / mol were selected as candidate drugs [23].

2.3 Visualization

Alignment between crystal structures and binding mode were visualized by Pymol 1.8 (https://pymol.org). Protein-ligand interaction pattern diagram was

shown by Discovery Studio 2016.

3. Results

By using high-throughput virtual screening, 23 approved drugs with binding energy below -11kcal / mol were obtained as candidate drugs (Fig. 1). The result included 7 peptides or peptide analogs and 17 small molecule drugs (Table 1 and Fig. 1). According to their characteristics, 10 out of 23 drugs were protease inhibitors, of which 9 drugs were HIV-1 protease inhibitors. It was suggested that the drug structure of the protease inhibitor was hit with a high probability.

3.1 3CL^{pro} amino acid sequence and structure analyses

By comparing the 3CL^{pro} structures of the two SARS-CoV-2 and SARS-CoV viruses, the secondary structure and tertiary structure of the two 3CL^{pro} did not change significantly near the crack between domains 1 and 2（Fig. S1A）. By analyzing amino acid sequence, their two 3CL^{pro}s reached 96% identity, and there were no significant changes in the main polar amino acids and charged amino acids (Fig. S1B and Fig. S2C). Based on the structure of 3CL^{pro} of SARS-CoV, homology modeling was performed. The model was compared with the crystal structure of 3CL^{pro} of SARS-CoV-2 and the results showed that the RMSD was 0.78 (Results not shown). It was shown that 3CL^{pro} of SARS-CoV-2 and 3CL^{pro} of SARS-CoV may have substantially the same catalytic mode. Therefore, drug candidates can be analyzed based on 3CL^{pro} related research experience on SARS-CoV.

3.2 Prediction of Ritonavir and Lopinavir

Currently, both Ritonavir and Lopinavir are used as a frontline treatment of COVID-19 and were found in the result of virtual screening (Fig. 2 and Fig. S5). They also have relatively consistent predicted binding energy (-11.8kcal / mol and -11.9kcal / mol, respectively).

3.3 Three protease inhibitors may outperform Ritonavir and Lopinavir

Among protease inhibitors, Carfilzomib (ZINC000049841054), Saquinavir (ZINC000003914596), and Indinavir (ZINC000022448696) have better docking scores (Fig. 1). As antitumor drug, Carfilzomib exerted its effect by binding to the active site of the 20S proteasome, which contained chymotrypsin whose spatial structure is like the $3CL^{pro}$. The docking results showed that the Carfilzomib was in $3CL^{pro}$'s pocket consisting of S1 and S2 subsites (Fig. 2A) and formed π-π stacking and hydrogen bonding with HIS-41 and CYS-145, respectively, in which were catalytic duplexes. The Carfilzomib also had multiple non-covalent interactions with MET-165 at the S1 subsite and MET-49 at the S2 subsite (Fig. 2B). Besides, both Saquinavir and Lopinavir had similar binding patterns (Fig. 3), and both stabilized HIS-41 and MET-49 in the same way. The non-covalent binding pattern of the Saquinavir and HIS-41 were similar to that of Carfilzomib, in which formed π-π stacks. The benzene ring interacted with MET-165 at the S3 subsite and MET-49 at the S2 subsite, and HIS-163 at the S2 subsite also formed a hydrogen bond interaction with Saquinavir. All three drugs formed hydrogen bonds with CYS-145. The results showed that Saquinavir and Lopinavir may have

similar mechanism. And docking scores of Indinavir and Lopinavir were almost the same, but the combination mode was less than Saquinavir (Fig. S4).

3.4 Good combination score of Peptidomimetic

The top three drugs with docking scores were peptides or peptide analogs (Table 1). Among them, Thymopentin got the highest score. It was able to bind $3CL^{pro}$'s substrate-binding pocket. Not only it can bind $3CL^{pro}$'s catalytic dyad Cys-145 and His-41, but also HIS-163, Glu166 at the S1 subsite and ASP-187 at the S2 subsite (Fig. 2A and B). It is well known that Thymopentin targets the lymphocytes as regulator in immune system, so it can be used for adjuvant treatment of viral infections. No inhibitory effect on proteases has been reported until we got the results of virtual screening.

3.5 Analyses of Other candidate drugs

Among non-protease inhibitor drugs, Viomycin, Cangrelor, Capastat, and Cobicistat also have higher predicted scores than Lopinavir. Two of them, Viomycin and Capastat are peptide analogs. Viomycin completely occupies the S1 subsite and binds to HIS-163, PHE-140, MET-165 and GLU-166. But it did not bind to His-41 and CYS-145 at the catalytic dyad (Fig. S2). Cangrelor can form hydrogen bonds with CYS-145 in the catalytic dyad, and effectively occupied the S1 and S3 subsites of $3CL^{pro}$ (Fig. S2). Capastat also binds well to the S1 and S3 subsites but no significant interaction with amino acids at the S2 subsite, and Hydrogen bonds with CYS-145 in the catalytic dyad (Fig. S3). Ceftolozane

interacts with the S1 subsite of 3CLpro and HIS-41 in the catalytic dyad (Fig. S3). Cobicistat was able to combine with the catalytic dyad of $3CL^{pro}$, and its combined poste was better than Indinavir (Fig. S4).

Among protease inhibitors, Telaprevir, Atazanavir, Darunavir, Nelfinavir, and Fosamprenavir were also selected to be candidates. However, their predicted binding power was weaker than that of the Lopinavir. Telaprevir mainly interacts with the catalytic dyad and has less interaction with the peptide binding site (Fig. S5).

In brief, the 23 approved drugs were identified to have the effect on inhibiting $3CL^{pro}$ by virtual screening. Among them, Ritonavir and Lopinavir have been currently used to treat COVID-19. And among the rest of 21 candidates, Carfilzomib, Saquinavir and Thymopentin showed more promising against SARS-CoV-2.

4. Discussion

The study is based on published data. For the limitations of our laboratory, further virus-related biological experiments cannot be allowed to carry out. So, we showed the disclosed data as reference for researchers and doctors in related fields.

In addition, considering the period of the drug development, the study only shows the information of 23 approved clinical drugs which obtained in the virtual screening. The other unapproved drug we got will be published if they will be investigated in the future biological experiments.

Moreover, since Carfilzomib's mechanism includes inhibition of chymotrypsin activity, it may better target $3CL^{pro}$ prospectively. In the prediction of binding energy and binding mode, Saquinavir showed similar results to Lopinavir, which can be further compared with the antiviral effect of Lopinavir. Although it is not reported that Thymic Pentapeptide has protease inhibitory activity, but it has predicted good inhibitory activity in the study. However, the Thymic Pentapeptide is composed of natural amino acids whereas $3CL^{pro}$ is a protease, so it is necessary to modify the structure to prevent excessive degradation of $3CL^{pro}$. Simultaneously, the study also referred that other candidates with potential $3CL^{pro}$ inhibitory activity might be as inhibitors of SARS-CoV-2.

We noticed Ritonavir / Lopinavir being clinically tested for the treatment of COVID-19 is an aspartate protease inhibitor. Their molecular structure is optimized for the aspartic protease spatial structure of HIV. But $3CL^{pro}$ is a cysteine protease. The difference in the spatial structure of $3CL^{pro}$ and HIV protease may lead to the actual inhibition efficiency. Hence, Ritonavir and Lopinavir are needed to further evaluate their effects when they resist SARS-CoV-2.

Acknowledgements

This work was supported by Operating Fund of Guangdong Provincial Key Laboratory of Bioengineering Medicine (NO.2014B030301050). We really appreciate that the Zihe Rao team of Shanghai Tech University shared the coordinate files of the $3CL^{pro}$ crystal structure for us to conduct the study. We also

thank that Miss. Marilou Ochivillo kindly gave language editing of the manuscript.

Conflict of interests

The authors declare no conflict of interests.

5. References

[1] M. Wang, R. Cao, L. Zhang, X. Yang, J. Liu, M. Xu, Z. Shi, Z. Hu, W. Zhong, G. Xiao, Remdesivir and chloroquine effectively inhibit the recently emerged novel coronavirus (2019-nCoV) in vitro, Cell Res, (2020).

[2] F. Touret, X. de Lamballerie, Of chloroquine and COVID-19, Antiviral Res, 177 (2020) 104762.

[3] P. Colson, J.M. Rolain, J.C. Lagier, P. Brouqui, D. Raoult, Chloroquine and hydroxychloroquine as available weapons to fight COVID-19, Int J Antimicrob Agents, (2020) 105932.

[4] J.F. Chan, Y. Yao, M.L. Yeung, W. Deng, L. Bao, L. Jia, F. Li, C. Xiao, H. Gao, P. Yu, J.P. Cai, H. Chu, J. Zhou, H. Chen, C. Qin, K.Y. Yuen, Treatment With Lopinavir/Ritonavir or Interferon-beta1b Improves Outcome of MERS-CoV Infection in a Nonhuman Primate Model of Common Marmoset, J Infect Dis, 212 (2015) 1904-1913.

[5] G. Li, E. De Clercq, Therapeutic options for the 2019 novel coronavirus (2019-nCoV), Nat Rev Drug Discov, 19 (2020) 149-150.

[6] C.M. Chu, V.C. Cheng, I.F. Hung, M.M. Wong, K.H. Chan, K.S. Chan, R.Y. Kao, L.L. Poon, C.L. Wong, Y. Guan, J.S. Peiris, K.Y. Yuen, H.U.S.S. Group, Role of lopinavir/ritonavir in the

treatment of SARS: initial virological and clinical findings, Thorax, 59 (2004) 252-256.

[7] K.S. Chan, S.T. Lai, C.M. Chu, E. Tsui, C.Y. Tam, M.M. Wong, M.W. Tse, T.L. Que, J.S. Peiris, J. Sung, V.C. Wong, K.Y. Yuen, Treatment of severe acute respiratory syndrome with lopinavir/ritonavir: a multicentre retrospective matched cohort study, Hong Kong Med J, 9 (2003) 399-406.

[8] F. Chen, K.H. Chan, Y. Jiang, R.Y. Kao, H.T. Lu, K.W. Fan, V.C. Cheng, W.H. Tsui, I.F. Hung, T.S. Lee, Y. Guan, J.S. Peiris, K.Y. Yuen, In vitro susceptibility of 10 clinical isolates of SARS coronavirus to selected antiviral compounds, J Clin Virol, 31 (2004) 69-75.

[9] M. Letko, A. Marzi, V. Munster, Functional assessment of cell entry and receptor usage for SARS-CoV-2 and other lineage B betacoronaviruses, Nat Microbiol, (2020).

[10] J. Cui, F. Li, Z.L. Shi, Origin and evolution of pathogenic coronaviruses, Nat Rev Microbiol, 17 (2019) 181-192.

[11] S. Perlman, J. Netland, Coronaviruses post-SARS: update on replication and pathogenesis, Nat Rev Microbiol, 7 (2009) 439-450.

[12] A. Zumla, J.F. Chan, E.I. Azhar, D.S. Hui, K.Y. Yuen, Coronaviruses - drug discovery and therapeutic options, Nat Rev Drug Discov, 15 (2016) 327-347.

[13] T. Pillaiyar, M. Manickam, V. Namasivayam, Y. Hayashi, S.H. Jung, An Overview of Severe Acute Respiratory Syndrome-Coronavirus (SARS-CoV) 3CL Protease Inhibitors: Peptidomimetics and Small Molecule Chemotherapy, J Med Chem, 59 (2016) 6595-6628.

[14] E. de Wit, N. van Doremalen, D. Falzarano, V.J. Munster, SARS and MERS: recent insights into emerging coronaviruses, Nat Rev Microbiol, 14 (2016) 523-534.

[15] W. Liu, J.S. Morse, T. Lalonde, S. Xu, Learning from the Past: Possible Urgent Prevention

and Treatment Options for Severe Acute Respiratory Infections Caused by 2019-nCoV, Chembiochem, (2020).

[16] C.C. Lee, C.J. Kuo, M.F. Hsu, P.H. Liang, J.M. Fang, J.J. Shie, A.H. Wang, Structural basis of mercury- and zinc-conjugated complexes as SARS-CoV 3C-like protease inhibitors, FEBS Lett, 581 (2007) 5454-5458.

[17] A. Waterhouse, M. Bertoni, S. Bienert, G. Studer, G. Tauriello, R. Gumienny, F.T. Heer, T.A.P. de Beer, C. Rempfer, L. Bordoli, R. Lepore, T. Schwede, SWISS-MODEL: homology modelling of protein structures and complexes, Nucleic Acids Res, 46 (2018) W296-W303.

[18] S. Bienert, A. Waterhouse, T.A. de Beer, G. Tauriello, G. Studer, L. Bordoli, T. Schwede, The SWISS-MODEL Repository-new features and functionality, Nucleic Acids Res, 45 (2017) D313-D319.

[19] W. Humphrey, A. Dalke, K. Schulten, VMD: visual molecular dynamics, J Mol Graph, 14 (1996) 33-38, 27-38.

[20] T. Sterling, J.J. Irwin, ZINC 15--Ligand Discovery for Everyone, J Chem Inf Model, 55 (2015) 2324-2337.

[21] H. Zhao, A. Caflisch, Discovery of dual ZAP70 and Syk kinases inhibitors by docking into a rare C-helix-out conformation of Syk, Bioorg Med Chem Lett, 24 (2014) 1523-1527.

[22] K. Anand, J. Ziebuhr, P. Wadhwani, J.R. Mesters, R. Hilgenfeld, Coronavirus main proteinase (3CLpro) structure: basis for design of anti-SARS drugs, Science, 300 (2003) 1763-1767.

[23] N. Zhang, H. Zhao, Enriching screening libraries with bioactive fragment space, Bioorg Med Chem Lett, 26 (2016) 3594-3597.

Figure Legends

Figure 1： Virtual screening results of drug candidates. Drugs were sorted according to the docking binding energy, corresponding to the order in Table 1. Unit：kcal/mol.

Figure 2: Binding patterns of thymopentin and carfilzomib to $3CL^{pro}$. (A and C) The three-dimensional binding modes of thymopentin and carfilzomib with 3CLpro, respectively. Protein shown as a cartoon model and ligands shown as stick model. (B and D) The interaction modes of both thymopentin and carfilzomib with $3CL^{pro}$, respectively.

Figure 3: Three-dimensional binding modes of saquinavir and lopinavir with $3CL^{pro}$. (A and C) The three-dimensional binding modes of saquinavir and lopinavir with $3CL^{pro}$, respectively. Protein shown as a cartoon model and ligands shown as stick model. (B and D) The interaction modes of both saquinavir and lopinavir with $3CL^{pro}$, respectively.

Figures/Tables

Table 1
Drug Candidate Information

Number	Drug	Molecular Type	Target	Indication
1	Thymopentin	Peptide	T lymphocyte	Viral infection
2	Viomycin	Peptidomimetic	Bacterial ribosomes	Bacterial infections
3	Carfilzomib	Peptidomimetic	20S Proteasome	Tumor
4	Cangrelor	Purine Nucleotides	P2Y12	Anticoagulation
5	Capastat	Peptidomimetic	Bacterial ribosomes	Bacterial infections
6	Saquinavir	Quinolines	HIV-1 Protease	HIV infection
7	Ceftolozane	Amides	PBPs	Bacterial infections
8	Cobicistat	Thiazoles	CYP3A	HIV infection
9	Indinavir	Pyridines	HIV-1 Protease	HIV infection
10	Lopinavir	Pyrimidinones	HIV-1 Protease	HIV infection
11	Ritonavir	Thiazoles	HIV-1 Protease	HIV infection
12	Telaprevir	Peptidomimetic	HIV-1 Protease	HIV infection
13	Plazomicin	Glycosides	Bacterial ribosomes	Bacterial infections
14	Mitoxantrone	Anthracyclines	DNA and topoisomerase II	Tumor
15	Macimorelin	Peptidomimetic	GHS-R1a	Growth hormone deficiency
16	FAD	Purine Nucleotides	Prosthetic	Adjuvant therapy
17	CoA	Purine Nucleotides	Coenzymes	Adjuvant therapy
18	Valrubicin	Anthracyclines	DNA and topoisomerase II	Tumor
19	Atazanavir	Peptidomimetic	HIV-1 Protease	HIV infection
20	Darunavir	Amides	HIV-1 Protease	HIV infection
21	Encorafenib	Amides	BRAF Kinase	Tumor
22	Nelfinavir	Isoquinolines	HIV-1 Protease	HIV infection
23	Fosamprenavir	Amides	HIV-1 Protease	HIV infection

Number	ZINC ID	Binding Energy	Vdw	Elec	H-bonding	Intraclash	Torsion
1	ZINC000003938642	-13.6	-59.52	2.1	-58.61	20.04	0.5
2	ZINC000049799668	-13.6	6.57	-16.93	-74.04	6.49	3.13
3	ZINC000049841054	-12.8	-53.81	-1.2	-44.6	12.97	5.76
4	ZINC000085537017	-12.6	-61	-2.5	-27.01	9.14	2.22
5	ZINC000150338698	-12.6	-16.15	-17.36	-63.33	7.08	4.33
6	ZINC000003914596	-12.4	-55.23	-6.1	-45.24	24.91	3.41
7	ZINC000009164421	-12.4	-48.57	-12.71	-49.22	4.8	0.73
8	ZINC000085537014	-12.3	-62.98	-0.7	-20.43	12.59	7.66
9	ZINC000022448696	-12	-51.42	-6.21	-32.24	3.81	3.23
10	ZINC000003951740	-11.9	-57	-1.08	-34.5	21.72	3.74
11	ZINC000003944422	-11.8	-55.39	-0.91	-27.57	7.16	4.92
12	ZINC000003992480	-11.8	-53.13	-1.5	-38.2	14.03	3.1
13	ZINC000068150640	-11.7	-49.3	-16.03	-40.14	23.37	3.5
14	ZINC000003794794	-11.6	-37.62	-13.88	-53.8	1.16	2.95
15	ZINC000001554197	-11.5	-41.66	-7.61	-43.21	0.07	1.67
16	ZINC000008215434	-11.4	-52.59	-1.4	-53.72	7.34	6.74
17	ZINC000008551087	-11.4	-59.13	2.62	-28.76	16.56	2.4
18	ZINC000163535243	-11.4	-42.81	-5.62	-30.82	2.4	1.63
19	ZINC000003941496	-11.1	-50.05	-0.85	-40.99	19.18	3.6
20	ZINC000003955219	-11.1	-51.76	-1.4	-19.38	6.54	1.97
21	ZINC000068249103	-11.1	-46.46	-0.72	-42.55	3.3	1.54
22	ZINC000003833846	-11	-46.91	-5.69	-25.85	3.52	2.23
23	ZINC000003941829	-11	-46.91	-5.69	-25.85	3.52	2.23

Figure 1

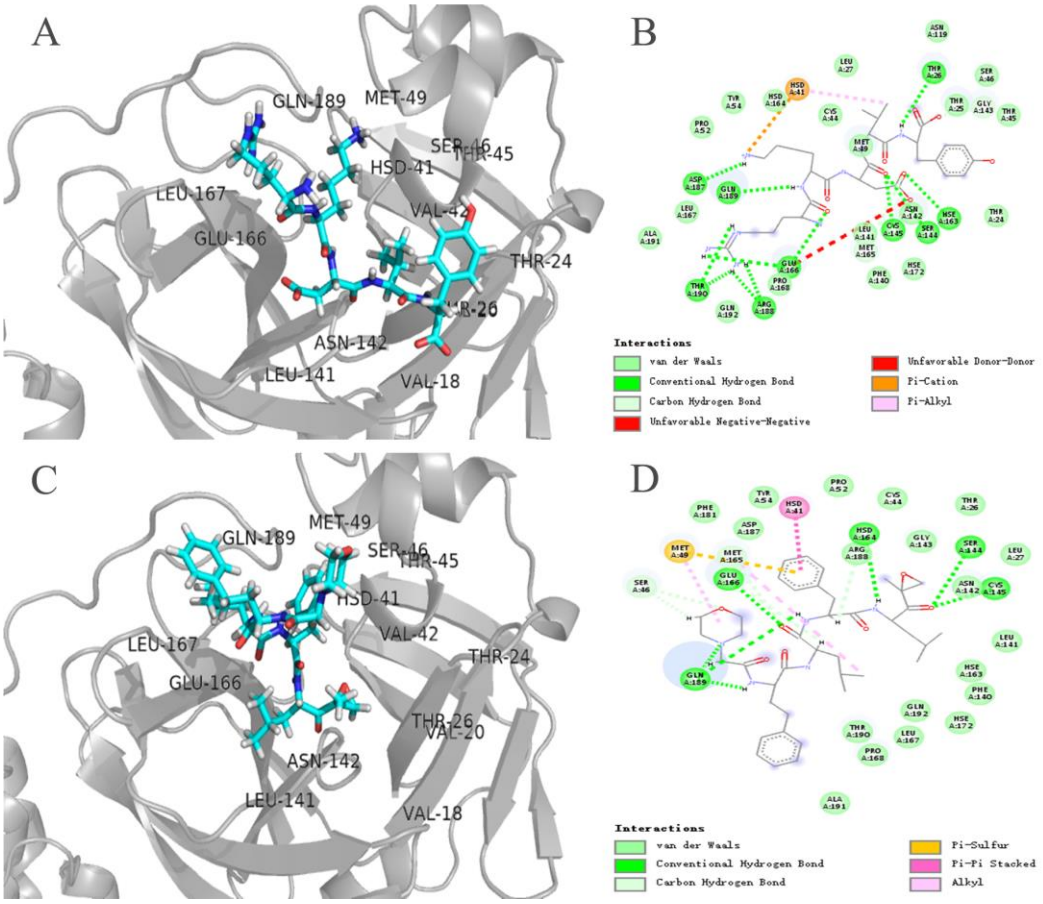

Figure 2

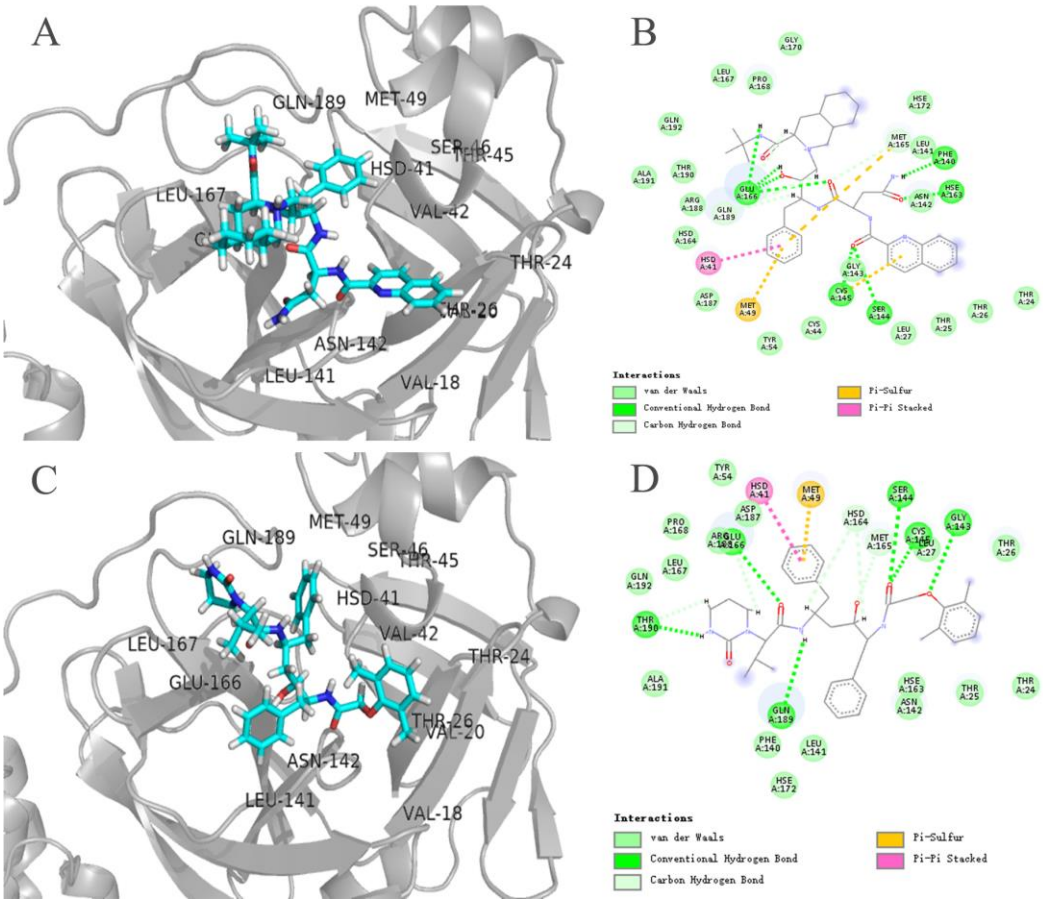

Figure3

Supplementary Material

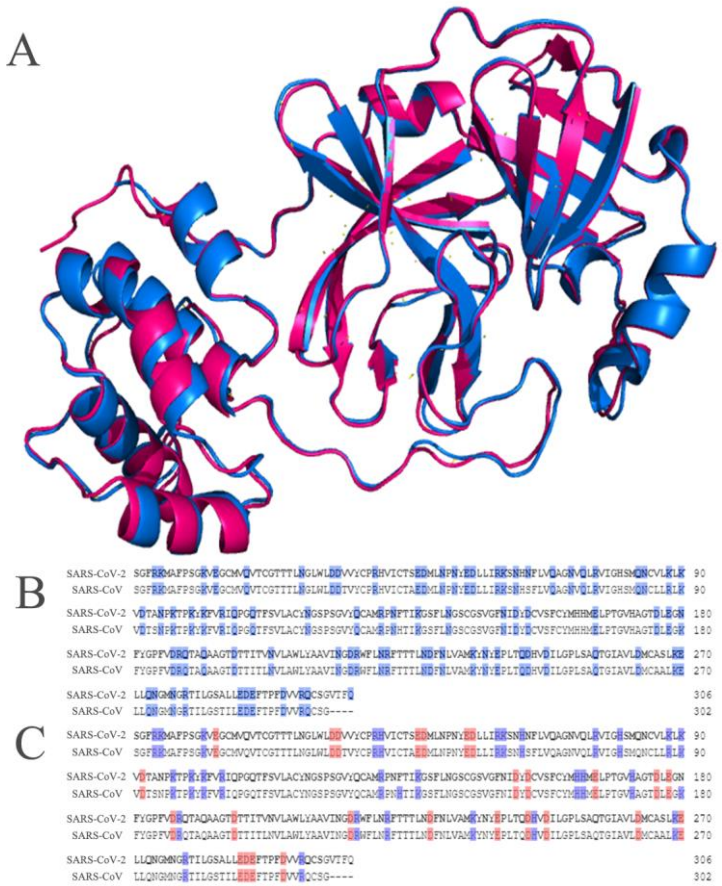

Figure S1: 3CL^{pro} amino acid sequence and structure analysis. (A) A comparison of two 3CL^{pro} structures of SARS-CoV and SARS-CoV-2. 3CL^{pro} of SARS-CoV （2Z9J） was shown in blue, and 3CL^{pro} of SARS-CoV-2（6LU7） was shown in red. (B) The 3CL^{pro} amino acid sequences of both SARS-Cov and SARS-CoV-2 were compared, and the polar amino acids were marked in blue. (C)Comparison of the 3CL^{pro} amino acid sequence of both SARS-Cov and SARS-CoV-2. Negatively charged amino acids were shown in red and positively charged amino acids are shown in red.

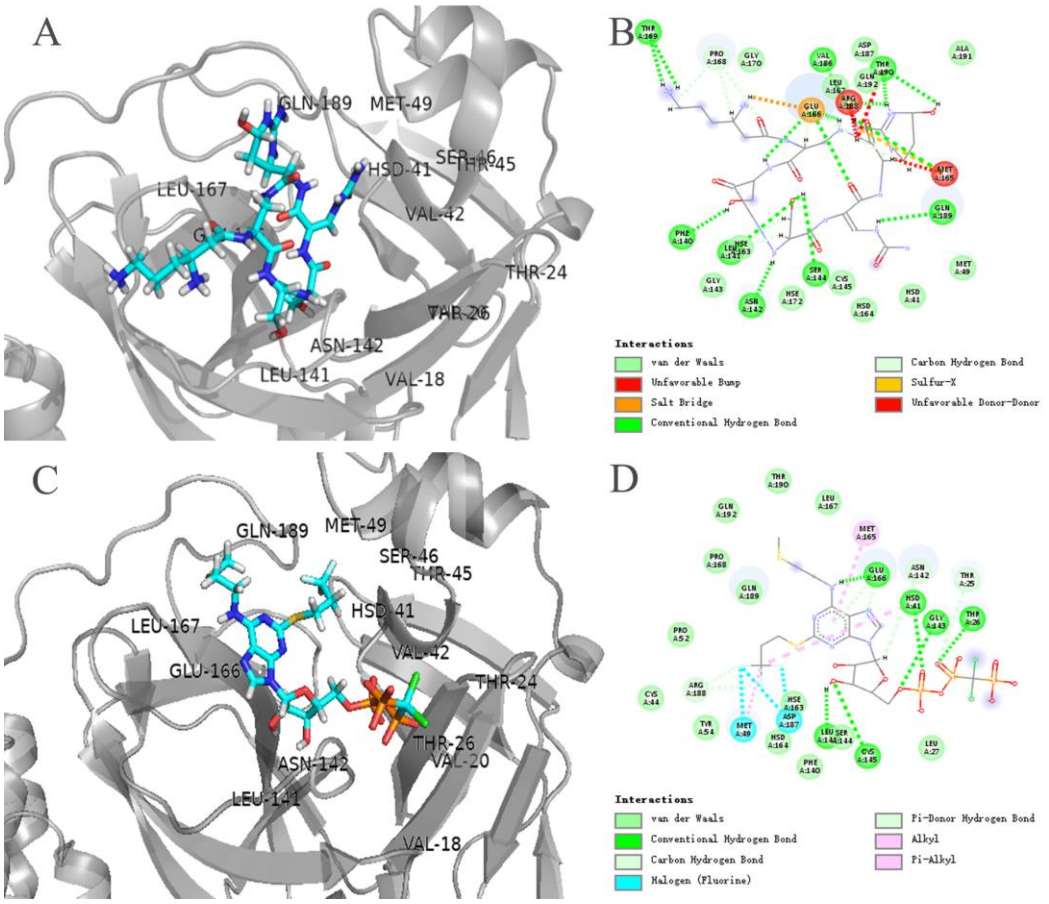

Figure S2: Three-dimensional binding modes of viomycin and cangrelor with $3CL^{pro}$. (A and C) The three-dimensional binding modes of both viomycin and cangrelor with $3CL^{pro}$, respectively Protein shown as a cartoon model and ligands shown as stick model. (B and D) The interaction modes of both viomycin and viomycin with $3CL^{pro}$, respectively.

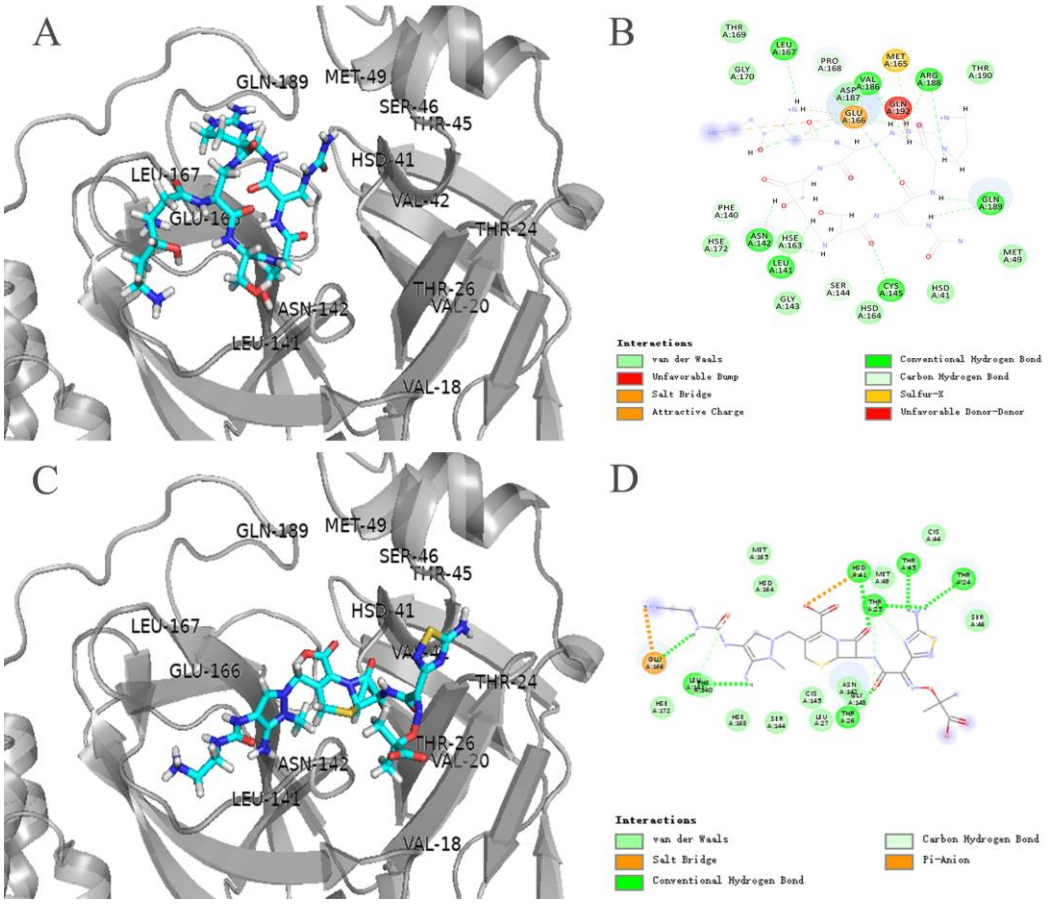

Figure S3: Three-dimensional binding modes of Capastat and Ceftolozane with 3CLpro. (A and C) The three-dimensional binding modes of both Capastat and Ceftolozane with $3CL^{pro}$, respectively. Protein shown as a cartoon model and ligands shown as stick model. (B and D) The interaction modes of both Capastat and Ceftolozane with $3CL^{pro}$, respectively.

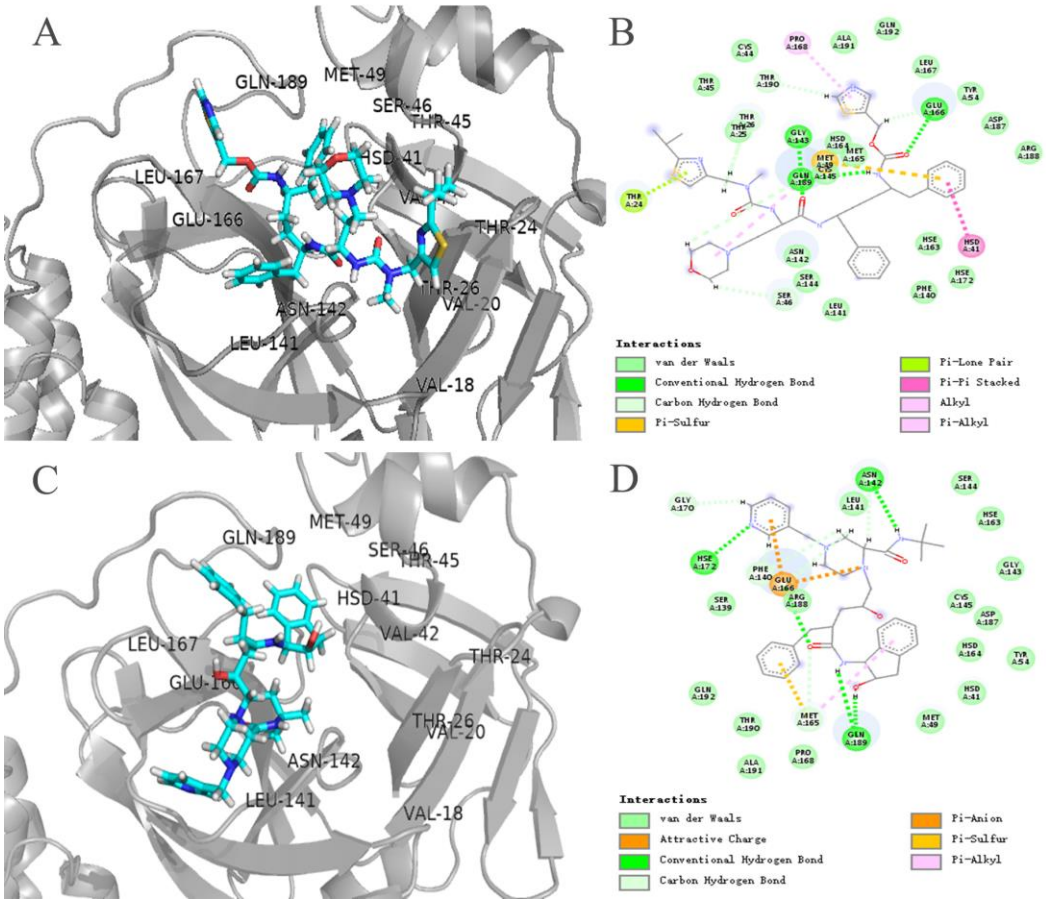

Figure S4: Three-dimensional binding modes of Cobicistat and Indinavir with $3CL^{pro}$. (A and C) The three-dimensional binding modes of both Cobicistat and Indinavir with $3CL^{pro}$, respectively. Protein shown as a cartoon model and ligands shown as stick model. (B and D) The interaction modes of both Cobicistat and Indinavir with $3CL^{pro}$, respectively.

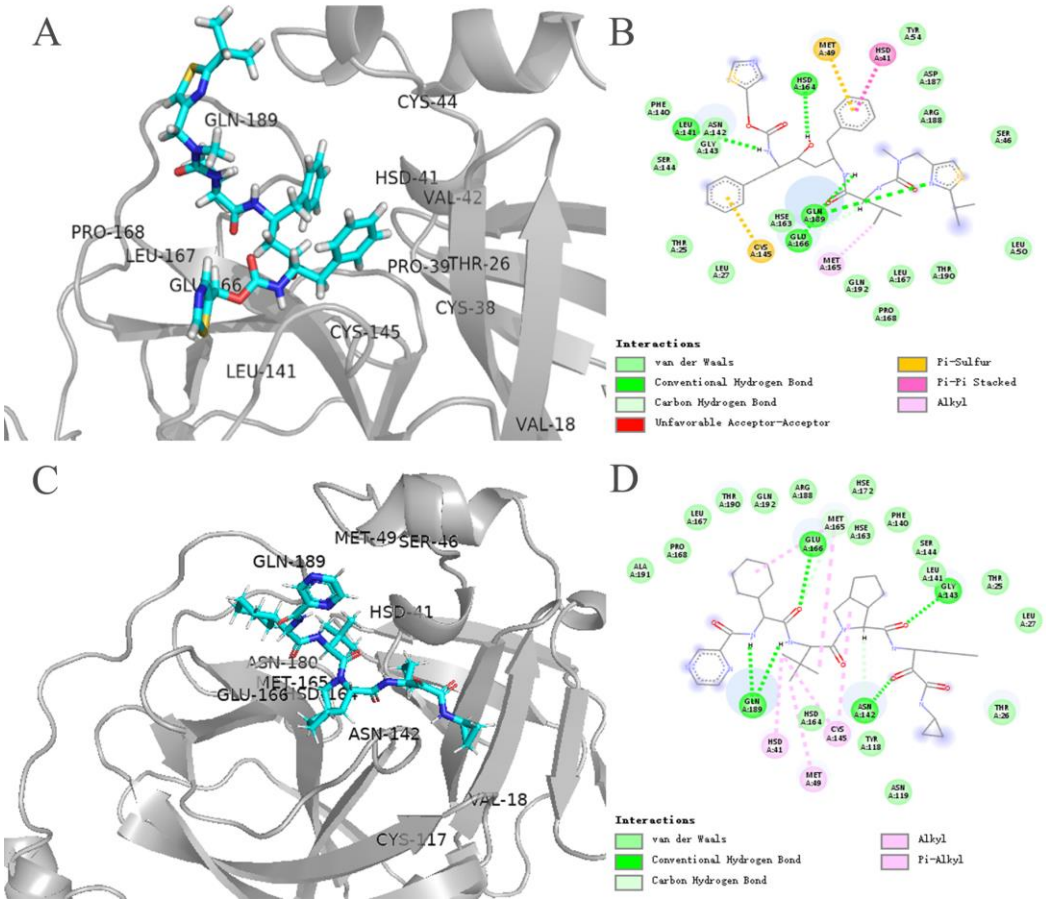

Figure S5: Three-dimensional binding modes of Ritonavir and Telaprevir with $3CL^{pro}$. (A and C) The three-dimensional binding modes of both Ritonavir and Telaprevir with $3CL^{pro}$, respectively. Protein shown as a cartoon model and ligands shown as stick model. (B and D) The interaction modes of both Ritonavir and Telaprevir with $3CL^{pro}$, respectively.